

OPEN

X-ray phase contrast imaging of *Vitis* spp. buds shows freezing pattern and correlation between volume and cold hardiness

Alisson P. Kovaleski^{1,2,3*}, Jason P. Londo^{1,2*} & Kenneth D. Finkelstein⁴

Grapevine (*Vitis* spp.) buds must survive winter temperatures in order to resume growth when suitable conditions return in spring. They do so by developing cold hardiness through deep supercooling, but the mechanistic process of supercooling in buds remains largely unknown. Here we use synchrotron X-ray phase contrast imaging to study cold hardiness-related characteristics of *V. amurensis*, *V. riparia*, and *V. vinifera* buds: time-resolved 2D imaging was used to visualize freezing; and microtomography was used to evaluate morphological changes during deacclimation. Bud cold hardiness was determined (low temperature exotherms; LTEs) using needle thermocouples during 2D imaging as buds were cooled with a N₂ gas cryostream. Resolution in 2D imaging did not allow for ice crystal identification, but freezing was assessed by movement of tissues coinciding with LTE values. Freezing was observed to propagate from the center of the bud toward the outer bud scales. The freezing events observed lasted several minutes. Additionally, loss of supercooling ability appears to be correlated with increases in bud tissue volume during the process of deacclimation, but major increases in volume occur after most of the supercooling ability is lost, suggesting growth resumption processes are limited by deacclimation state.

Grapevines (*Vitis* spp.) produce compound mixed buds that contain both vegetative and reproductive tissue in a primary bud, and predominantly vegetative tissue in secondary and tertiary buds¹. These buds are produced during the growing season, and transition into a dormant state to survive unsuitable growth conditions, such as drought or low temperature. Throughout the winter, grapevine buds will remain dormant and develop cold hardiness in order to prevent damage from low temperatures. Winter dormancy status is transitional, subtly changing from an endodormant to ecodormant status. During endodormancy, buds are recalcitrant to growth due to mostly unknown internal regulation. However, upon progressive chill accumulation, buds become ecodormant and will resume growth if exposed to permissive conditions².

Growth resumption under forcing conditions, marked by the appearance of budbreak (e.g., opening of outer scales and emergence of tissue from the bud), is typically used to evaluate the changes in dormancy level that occur during winter^{3,4}. However, this comparison of phenological stage is dependent on comparable development between genotypes or species: if growth and expansion in the bud during dormancy release is not the same in all genotypes, we could incorrectly describe the relationship of cold hardiness and budbreak phenology. For example, phenological scales for budbreak in grapevine are based on observations of *V. vinifera* buds^{5,6}, the most widely cultivated grapevine species, and may incorrectly describe changes that occur in wild species. Recently, this dormancy transition has been observed through gradual increases in rate of cold hardiness loss (deacclimation rate) that occurs with chill accumulation over the winter season⁷, although the cold hardiness level *per se* and dormancy are independent. However, the relationship between the kinetics of the deacclimation process and budbreak is different for species within *Vitis*: buds of cultivated grapevine (*V. vinifera*) only begin showing a budbreak phenotype after the majority of the cold hardiness is lost, whereas buds of *V. riparia* may present budbreak prior to fully losing their cold hardiness⁷. Therefore, exploring differences in morphological aspects of

¹School of Integrative Plant Science – Horticulture Section, Cornell University – Cornell AgriTech, Geneva, NY, USA.

²United States Department of Agriculture, Agricultural Research Service, Grape Genetics Research Unit, Geneva, NY, USA. ³The Arnold Arboretum of Harvard University, Boston, MA, USA. ⁴Cornell High Energy Synchrotron Source, Cornell University, Ithaca, NY, USA. *email: ap874@cornell.edu; jason.londo@usda.gov

Vitis species buds during deacclimation may elucidate important differences in time to budbreak and its relation to deacclimation kinetics.

While the majority of methods for studying bud morphology is destructive (e.g., sectioning), non-destructive methods may give better insight into how the developmental process of early budbreak affects the perception of phenological progression. Tomography imaging is an underused technique in plant sciences⁸ that may be an alternative for the study of morphological differences between buds. This technique has recently become a consolidated method for the study of xylem and wood characteristics^{9–17}, but other plant structures have also been imaged, such as developing maize seeds¹⁸, tomato leaves¹⁹, and flowers and floral buds^{8,20}.

Developmental changes may justify differences between species for budbreak and deacclimation, but questions still remain in regard to the cold hardiness phenotype itself. Dormant buds of woody species experience temperatures below the freezing point of water during the winter in higher latitudes, and as a consequence have developed strategies to prevent bud death. Grapevine buds, as well as a number of other woody perennials, survive these low temperatures and gain cold hardiness by promoting the supercooling of water in tissues^{21–23}. Through this process, pure water can remain liquid to temperatures close to -42°C ²⁴. If the bud cold hardiness threshold is surpassed by low temperatures, bud mortality ensues, impairing growth and flowering in the following season. The maximum cold hardiness levels achieved (i.e., the minimum temperature buds may survive) are different for different species, ranging from high negative temperatures (i.e., -7°C) to very close to the $\sim -42^{\circ}\text{C}$ supercooling limit²³. Within grapevines, bud cold hardiness changes throughout the winter, primarily driven by changes in air temperature^{7,25–27} and there is variation among species and cultivars within a species. Maximum cold hardiness has been observed to be mostly between -24°C and -35°C ^{22,25–27}, with cultivated varieties being less cold hardy than wild species. Although low temperatures are the most limiting factor in plant distribution²⁸, the process through which plants control the supercooling point of buds and other structures remains largely unknown.

Damage in grapevine buds when supercooling fails is hypothesized to occur from the formation of intracellular ice^{22,29}, however location of ice nucleation has not been studied in grapevines. The observation of the freezing process is the best means for understanding how the event causes damage³⁰ and the identification of regions of the bud where supercooling fails can help understanding how plants control supercooling. Multiple techniques have been used to observe or infer ice formation in food and biological samples: indirect observation through freeze-substitution, identifying holes left in tissues by ice;³¹ light microscopy;^{30,32–36} fluorescence microscopy with the aid of a microslicer for 3D ice structure;³⁷ NMR microscopy;^{38,39} freeze fracture Cryo-SEM;^{35,36} infrared imaging,^{40–44} and confocal laser scanning microscopy⁴⁵. In plants, Endoh *et al.*³⁵ used light microscopy to examine extracellular ice crystals and freeze fracture Cryo-SEM to evaluate the presence of intracellular ice, based on the presence of crystalline ice vs. amorphous ice inside cells in buds of larch (*Larix kaempferi*). These methods, however, do not allow for temporal imaging of ice fronts. Using time-resolved X-ray phase contrast imaging, Sinclair *et al.*⁴⁶ observed the growth of ice crystals in insect larvae in real time. X-ray phase contrast imaging of freezing appears to be an interesting option for imaging freezing in buds, considering the opaque nature of the structure, as well as the fact that it allows for temporal imaging of ice spreading⁴⁶.

Understanding morphological changes within buds during deacclimation, as well as where freezing occurs may provide new insights into dormancy release and plant control over supercooling ability. Therefore, the objective of this study was to evaluate morphological development of buds from different *Vitis* species during loss of hardiness and budbreak, and image the freezing of buds to identify regions of the bud where the supercooling mechanism fails using X-ray phase contrast imaging. For this comparison, we used species from three major clades in *Vitis* (Asian: *V. amurensis*; North American: *V. riparia*; and Eurasian: and *V. vinifera*⁴⁷) which had been previously compared in studies of the kinetics of deacclimation⁷ and gene expression during deacclimation⁴⁸.

Methods

Plant material and cold hardiness. Buds of *V. amurensis* PI588641, *V. riparia* PI588711, and *V. vinifera* ‘Riesling’ were collected from the field on 31 January 2018, prepared into single node cuttings and placed in a 4°C cold room in cups of water. In preparation for imaging, sets of buds were removed from the cold room and placed under forcing conditions (22°C , 16 h/8 h light/dark) periodically to deacclimate. Buds were removed on 31 Jan, 2 Feb, 5 Feb, 7 Feb, and 11 Feb 2018 for *V. riparia* and *V. vinifera*; and 8 Feb and 11 Feb 2018 for *V. amurensis*. On 13 Feb 2018, cold hardiness of buds was determined and buds were moved back into cold room (4°C), where they were maintained throughout the imaging period to minimize changes in cold hardiness and developmental stage⁷. This sampling scheme provided us with buds at 0, 2, 6, 8, 11, and 13 days of deacclimation for *V. riparia* and *V. vinifera*, and 0, 2, 5 days for *V. amurensis*.

Cold hardiness was determined through differential thermal analysis (DTA), as represented by individual low temperature exotherm (LTE) of buds²⁹. In summary, buds are excised from cane and placed on thermoelectric modules (TEM) in plates, which are then placed in a programmable freezer. The freezer is cooled at -4°C hour^{-1} , and changes in voltage due to release of heat by freezing of water is measured by the TEMs and recorded via Keithley data logger (Tektronix, Beaverton, OR) attached to a computer. Deacclimation rates were estimated using linear regression⁷ using R (ver. 3.3.0, R Foundation for Statistical Computing). R was also used to produce all plots.

X-ray phase contrast imaging. Buds attached to a piece of cane were held on a custom-made cylindrical holder with mounting putty. The holder was attached to a small goniometer mounted on a Huber 4-circle diffractometer. Imaging was performed in the C-line at the Cornell High Energy Synchrotron Source (CHESS, Cornell University, Ithaca, USA). The monochromatic beam was expanded to $7\text{ mm} \times 7\text{ mm}$ at X-ray energy 15 KeV. The sample-detector distance used was optimized to 0.5 m. Phase-contrast is produced when majority unperturbed beam interferes with angular deviations in the wavefront caused by density variations in the sample⁴⁹. X-rays were

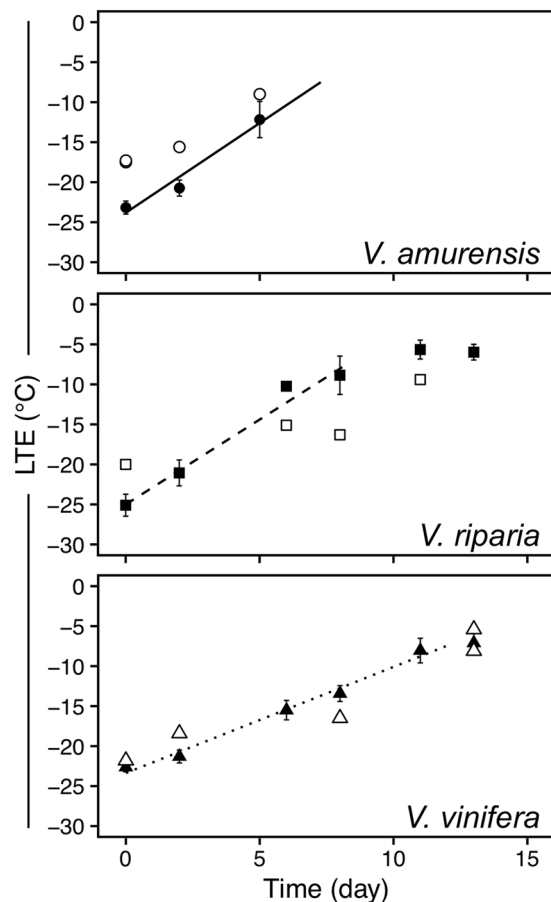


Figure 1. Deacclimation of *Vitis amurensis*, *V. riparia*, and *V. vinifera* ‘Riesling’ under forcing conditions. Full symbols represent average bud cold hardiness estimated through differential thermal analysis (DTA), while open symbols represent freezing temperature of single buds under a cryostream. Error bars represent standard deviation of the mean. Deacclimation rates (linear regression) were $2.24^{\circ}\text{C day}^{-1}$ ($R^2 = 0.89$), $2.12^{\circ}\text{C day}^{-1}$ ($R^2 = 0.92$), and $1.33^{\circ}\text{C day}^{-1}$ ($R^2 = 0.95$) for *V. amurensis*, *V. riparia*, and *V. vinifera*, respectively ($P < 0.001$ for all), at 22°C and 16h/8h light/dark. For *V. riparia* and *V. vinifera* rates were calculated from day 0 to days 8 and 11, respectively.

converted into visible light using a rare-earth doped GGG ($\text{Gd}_3\text{Ga}_5\text{O}_{12}$) crystal plate and imaged using an Andor Neo CMOS camera (detector pixel size $6.5\ \mu\text{m}$) with a 5x objective lens.

For morphological changes in buds, tomographic-like imaging was performed with camera resolution of approximately $5\ \mu\text{m}$, obtained by adjusting magnification of the objective lens. Buds were scanned while rotating over 180° , with images collected every $\frac{1}{4}$ or $\frac{1}{2}$ degree. Reconstruction of bud structure based on these datasets was performed using Octopus Reconstruction software (ver. 8.8.1, Inside Matters, Belgium). After reconstruction, buds were visualized in 3D using OsiriX imaging software (ver. 8.0.1, Pixmeo, Switzerland). For volume measurements, a threshold was visually established for each bud to remove noise and background. The bud cushion (i.e., undifferentiated tissue connecting bud to shoot) was removed from the image, and only the bud itself was used. Volume was determined by counting the number of voxels in the 3D image using the ROI tool within OsiriX. Volume was observed as percent increase in volume (ΔV) from the sample in day 0. If more than one bud was imaged for day 0, the average volume of samples was used as the base value – but individual measurements are displayed for any day.

Freezing of the buds was observed using 2D time-lapse imaging with images at $2\ \mu\text{m}$ pixel size, and was performed in the same buds used for 3D imaging. A 1 second exposure was used, but image capturing time effectively resulted in 0.56 Hz frequency. During the imaging, buds were cooled using a N_2 gas cryostream (Oxford Cryosystems, UK), with a constant cooling rate of $\sim -40^{\circ}\text{C hour}^{-1}$. A thermocouple in a 33-gauge needle probe (Omega Engineering, Inc., USA) was inserted in the bud during imaging and used to measure the temperature inside the bud, and temperature measurements were recorded using an RDXL4SD data logger (Omega Engineering, Inc., USA). LTEs for these samples were observed as temperature deviations from the linear rate of cooling. Contraction of the mounting putty due to cooling resulted in a slow downward drift of the bud, therefore image sets were aligned using the Linear Stack Alignment with SIFT plugin (https://imagej.net/Linear_Stack_Alignment_with_SIFT;⁵⁰) in Fiji (ImageJ ver. 2.0.0;⁵¹), and then cropped to remove black edges. Kymographs were obtained from the aligned image stacks using Fiji. To evaluate changes in buds over time, as sample is

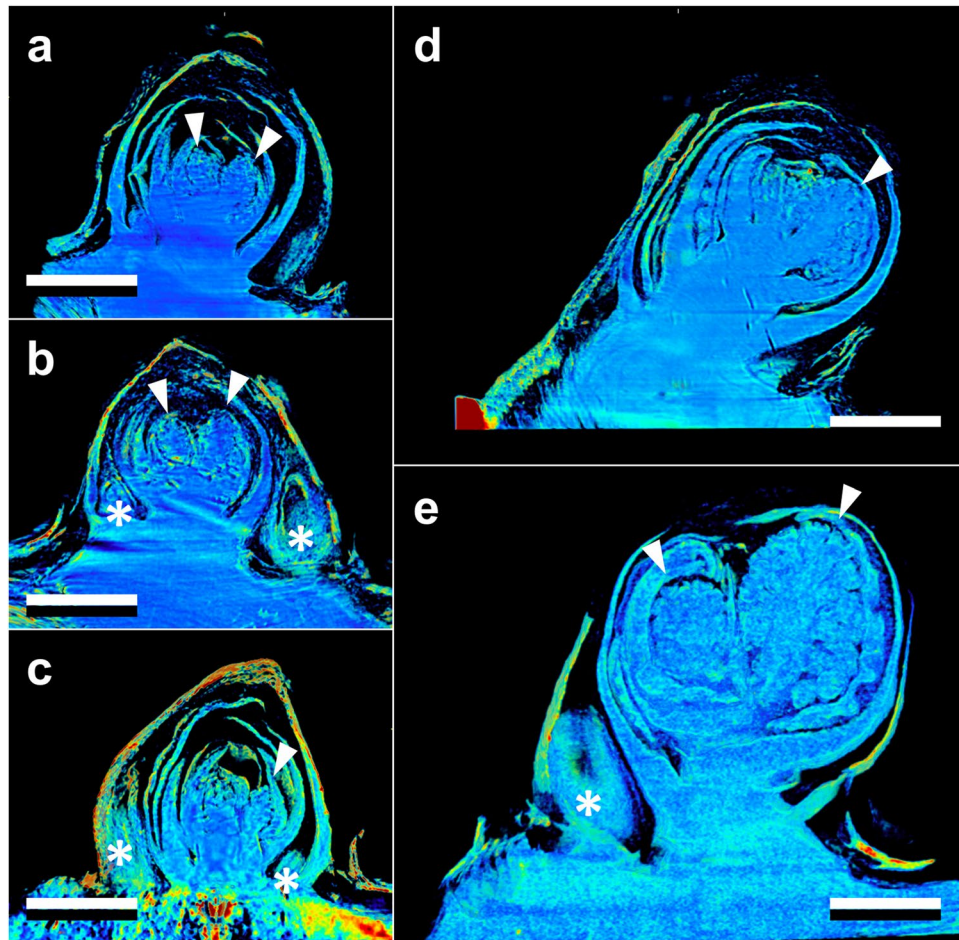


Figure 2. Development of *Vitis riparia* buds during budbreak reconstructed using X-ray microtomography. Buds shown were imaged at 0 (a), 2 (b), 8 (c), 11 (d), and 13 (e) days under forcing conditions. Full arrow heads indicate inflorescences, asterisks indicate secondary and tertiary bud. Scale bar = 1 mm (all images are in the same scale).

being cooled at constant rate, multi-scale structural similarity (MS SSIM) index⁵² was quantified between each image and the initial image in each sequence using the MS SSIM index plugin (<https://imagej.nih.gov/ij/plugins/mssim-index.html>) in Fiji. To compare different regions of the buds, MS SSIM index values were normalized to a maximum of 100% (most similar to initial image) and minimum of 0% (least similar). Image stacks were transformed into videos using Fiji, and temperature and image information were matched using time stamps in data-logger and images, added using the *Series Labeler* plugin (https://imagej.net/Series_Labeler). The time required to image buds for 3D scans and freezing scans limited the number of repetitions imaged.

Results

Deacclimation of the buds was well described by linear behavior until the limits of detection of LTEs (Fig. 1). For *V. amurensis* all data points were used, whereas for *V. riparia* and *V. vinifera* data points through day 8 and 11 were used for rate calculation, respectively. *V. amurensis* and *V. riparia* had similar deacclimation rates, at $2.2^{\circ}\text{C day}^{-1}$ ($R^2 = 0.89$) and $2.1^{\circ}\text{C day}^{-1}$ ($R^2 = 0.92$), respectively. *V. vinifera* had a lower deacclimation rate, at $1.3^{\circ}\text{C day}^{-1}$ ($R^2 = 0.95$). LTEs determined using needle probes inserted in the buds during imaging of freezing produced similar results to those using the regular DTA method.

Both the vegetative and reproductive aspects of the mixed *Vitis* bud structure were visible in micro-CT imaging (Figs 2–4). As a consequence of faster deacclimation and development, *V. riparia* buds were imaged through a wider range of developmental stages (Fig. 2) than *V. vinifera* (Fig. 3). *V. riparia* was imaged in E-L stages 1 – “winter bud” (Fig. 2a–c), 2 – “bud scales opening” (Fig. 2d), and 3 – “wooly bud” (Fig. 2e). *V. vinifera* buds have an outer appearance of E-L stage 1 in Fig. 3a–c, and is at an early stage 2 in Fig. 3d. With a reduced number of sampling dates, *V. amurensis* buds were all at E-L stage 1 and had the lowest range of development imaged (Fig. 4). Primary, secondary, and tertiary buds are visible in the still images shown for all three species. Images provide clear identification of inflorescences in the primary bud, even in the fully dormant state (day 0; Figs 2a, 3a and 4a).

Clear morphological differences can be seen when comparing buds of the different species. *V. riparia* buds are much smaller than *V. vinifera* and *V. amurensis*. The inflorescence primordia in *V. riparia*, however, take up much

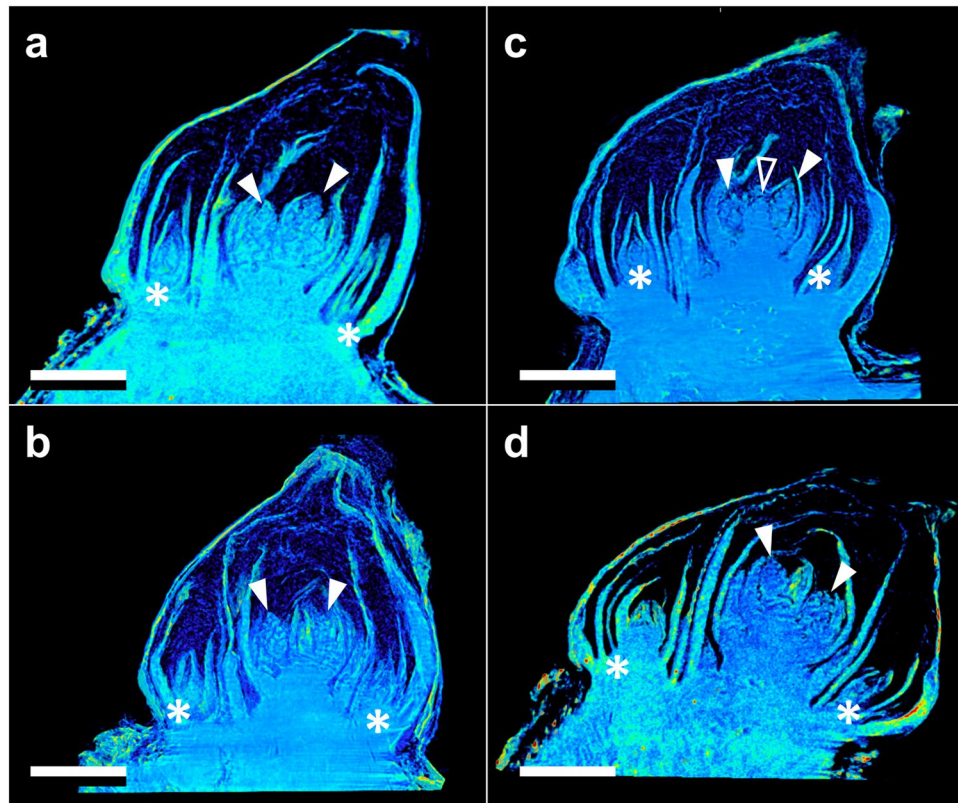


Figure 3. Development of *Vitis vinifera* buds during budbreak reconstructed using X-ray microtomography. Buds shown were imaged at 0 (a), 2 (b), 8 (c), and 13 (d) days under forcing conditions. Full arrow heads indicate inflorescences, open arrow head indicates apical meristem, asterisks indicate secondary and tertiary bud. Scale bar = 1 mm (all images are in the same scale).

more of the volume of day 0 buds in *V. riparia* than in *V. vinifera*. Both *V. vinifera* and *V. riparia* have inflorescence primordia of ~0.5 mm, whereas in *V. amurensis* they are ~1 mm long and appear more developed. Buds of *V. vinifera* have much more space between the leaf primordia, inflorescence primordia, and the outer bud scales compared to the two other species, especially *V. amurensis*. This space is occupied by “wool” or “hair”, most visible in Fig. 3b,c. *V. amurensis* buds are very compact at the dormant stage, and there is very little space between the scales and leaf primordia, which can be seen folding down on the top, as if constrained by the outer scales (Fig. 4a).

In *V. riparia*, there are very little differences in morphology between the buds until day 8 (Fig. 2a–c). However, once LTE values were above -10°C [close to the limit of detection where high temperature exotherms (HTEs) and LTEs may combine in DTA; Fig. 1], a noticeable increase in the bud size can be observed (Figs 2d,e and 5). Much of this change appears to be due to the expansion and development of the inflorescence primordia, and elongation of the base of the primary bud (shoot). In *V. vinifera*, the inflorescence primordia appear to remain the same size as the buds lose hardness but there is a noticeable expansion of the base of the primary bud. In *V. amurensis*, there are no clear internal differences seen between day 0 and 5.

The visual assessments of expansion in bud tissues are confirmed by analysis of the volume of tissue (ΔV) in the buds (Fig. 5). *V. riparia* buds reached the greatest expansion in volume within the time analyzed, reaching at day 13 almost triple the size of buds in day 0. *V. amurensis* appears to have a similar slope when the first days are considered compared to *V. riparia*, while *V. vinifera* has the slowest increase in bud volume. Both *V. riparia* and *V. vinifera* buds had increased ~50% in volume when most of the hardness was lost (day 8 and day 13, respectively), although the rate of volume increase is much higher after all cold hardness is lost for *V. riparia* (day 8–13). Pearson’s correlation for the relationship between LTE (open symbols in Fig. 1) and ΔV for *V. amurensis*, *V. riparia* and *V. vinifera* are 0.94, 0.96 and 0.96, respectively.

Freezing of the buds occurred from the inside-out (Figs 6 and 7, Supplementary Videos S1–S3). The videos are produced based on projection images that show the accumulated structure of buds (i.e., no depth resolution; Fig. 6a same bud as in Fig. 2d; and Fig. 7a same bud as in Fig. 4a). Freezing in this *V. riparia* bud is observed at $-9.4^{\circ}\text{C}/28:41\text{ mm:ss}$ (Supplementary Video S1). In a kymograph taken through the mid-section of the bud, an expansion of tissues is visualized by the drift outward in the structures – showing a positive slope on the right side of the bud (top of Fig. 6b) and a negative slope on the left side (bottom of Fig. 6b). The MS SSIM is a measure of the similarity in distribution of pixels between two images (Fig. 6c). When aligning the MS SSIM and temperature probe data (Fig. 6c,d), we observe that there is a slow decay in MS SSIM during the initial cool down. Such slow decay is a combination of appearing structures due to scratches in the crystal used to expand the beam and small inaccuracies in the linear alignment of the stack. The fastest decay in MS SSIM, however, occurs simultaneously

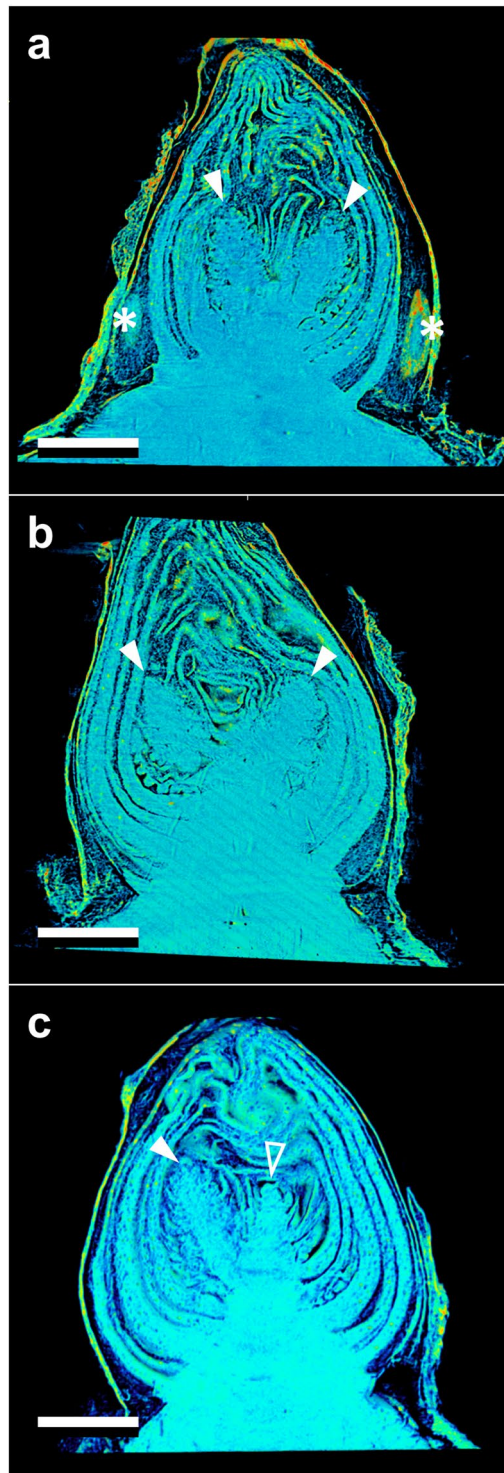


Figure 4. Development of *Vitis amurensis* buds during budbreak reconstructed using X-ray microtomography. Buds shown were imaged at 0 (a), 2 (b), and 5 (c) days under forcing conditions. Full arrow heads indicate inflorescences, open arrow head indicates apical meristem, asterisks indicate secondary and tertiary bud. Scale bar = 1 mm (all images are in the same scale).

with the recording of increase in temperature due to heat release of water freezing, meaning that pixels are being displaced from their initial location at a fast rate. When comparing different sections of the bud, the MS SSIM index decays to a minimum value earlier in the center section than in the top (Fig. 6c inset). In a *V. amurensis* bud from day 0 (Fig. 4a), freezing of the primary bud occurred at -17.5°C [Fig. 7d; Supplementary Video S2 (time-stamp 32:10)]. The freezing resulted in an increase in the inner temperature of the bud of $\sim 8^{\circ}\text{C}$, reaching -9.4°C . A much smaller increase in temperature occurs at 39:14, caused by the freezing of secondary bud. The

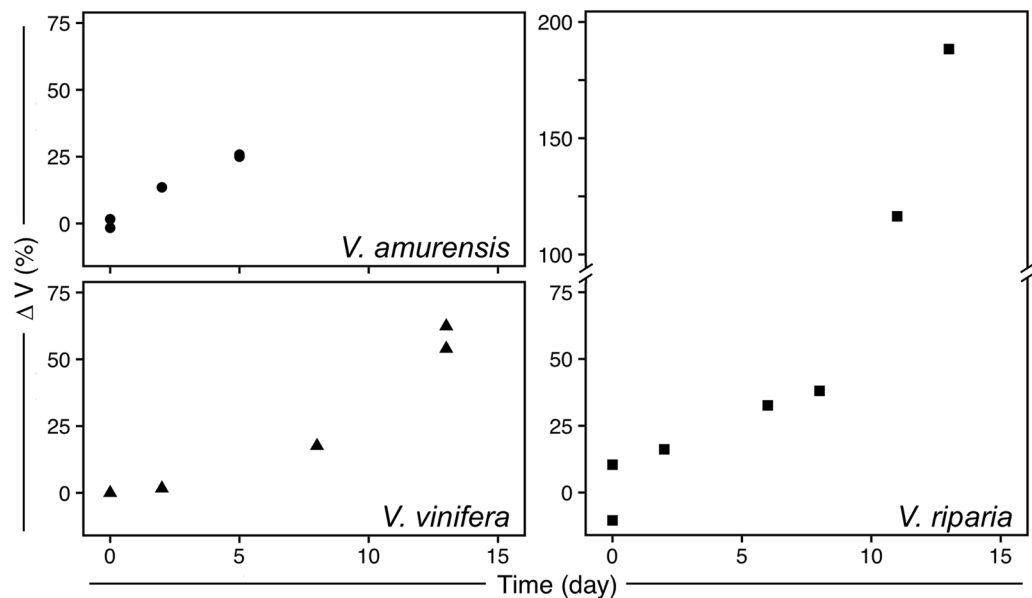


Figure 5. Increase in volume (ΔV) of *Vitis amurensis*, *V. riparia*, and *V. vinifera* during deacclimation. Volume was determined by counting the number of voxels in X-ray microtomography-reconstructed buds, therefore not including air space. ΔV was calculated as the percent increase in volume from sample (or average of samples) at day 0. Each point represents an individual sample.

position of the bud and size of the secondary hinder our ability to detect where the freezing originates, although it appears to be an independent event from that of the primary bud freezing. Evaluation of kymograph for *V. amurensis* shows a subtler frameshift caused by expansion (Fig. 7b), but MS SSIM results for *V. amurensis* (Fig. 7c) are very similar to those for *V. riparia*. Detection of freezing in *V. vinifera* was subtler, with a very slight expansion of the center portion of the bud [Supplementary Video S3 (−18.3°C/33:30)]. The movement of tissues that signals freezing can be observed occurring over minutes in all genotypes: between 28:41 and ~34:00 in *V. riparia*, 32:10 to ~41:00 in *V. amurensis*, and 33:30 to ~36:00 in *V. vinifera*.

Discussion

Only recently has X-ray microtomography begun to be used for the exploration of floral development in annual plants²⁰ (and referencing papers), but here we demonstrate the use of this technique to study morphological changes in buds of woody perennials. More importantly, we used quantitative data derived from tomography scans to explore concepts related to cold hardiness, and X-ray phase contrast imaging to visualize freezing. We demonstrate that small gains in volume occur during deacclimation, but increases are much faster once most of the supercooling ability of buds is lost, suggesting that the ability to supercool to low temperatures – be that on its own or as another effect of the processes that control the supercooling levels – in some way limits growth and development in dormant grapevine buds. Although the freezing method and rate of cooling were different than that typically used, the use of temporal X-ray imaging clearly shows that the freezing of tissues occurs from the inside of the bud and propagates to the outside, and that the freezing of bud tissues can last several minutes.

The non-destructive nature of X-ray phase contrast imaging is an interesting aspect for study of supercooling in buds, where damage to the structure of the bud can result in no detection of LTEs⁵³. Although long-term survivorship of the buds was not tested, and radiation levels could potentially lead to cell death^{46,49}, buds that were imaged showed LTEs in comparable levels to those determined in standard DTA analysis (open vs. full symbols in Fig. 1, respectively), even those that were almost fully deacclimated (e.g., *V. riparia* bud in Fig. 6 and Supplementary Video S1). This demonstrates that at least for a few hours (scan for 3D imaging was ~1 h, followed by the freezing scan) the buds remained viable, as dead buds show no, or much warmer, LTEs. This also demonstrates that the thermocouple probes in the needles are effective for the detection of exotherms related to cold hardiness of buds, and that placement of needles did not disrupt usual supercooling. The comparable LTE levels are very interesting considering two aspects: (i) the high rate of cooling used and (ii) the lack of observed HTEs. The rate of cooling used in the cryostream was ~10x higher than that normally used in DTA – including DTA measurements used here to determine initial cold hardiness. The higher rate was required due to the time constrains for beam access, and faster freezing allowed us to image a greater number of buds. While the rates of cooling at the level used in this study reportedly cause a decrease in LTE temperature (more negative) of *V. vinifera* hybrid grapevines⁵⁴, higher rates of cooling result in freezing at warmer temperatures for *Rhododendron* spp.⁵⁵. We did not observe a particular trend when all species are taken into account. However, all the buds of *V. amurensis* froze at higher temperatures than expected. This is likely a result of the over 2x greater rate of deacclimation this species has compared to the other two at low temperatures⁷, and therefore storage may have resulted in some cold hardiness loss. In addition, high levels of bud damage in *V. amurensis* in field conditions also reduced the number of buds available for analysis, reducing the number of data points.

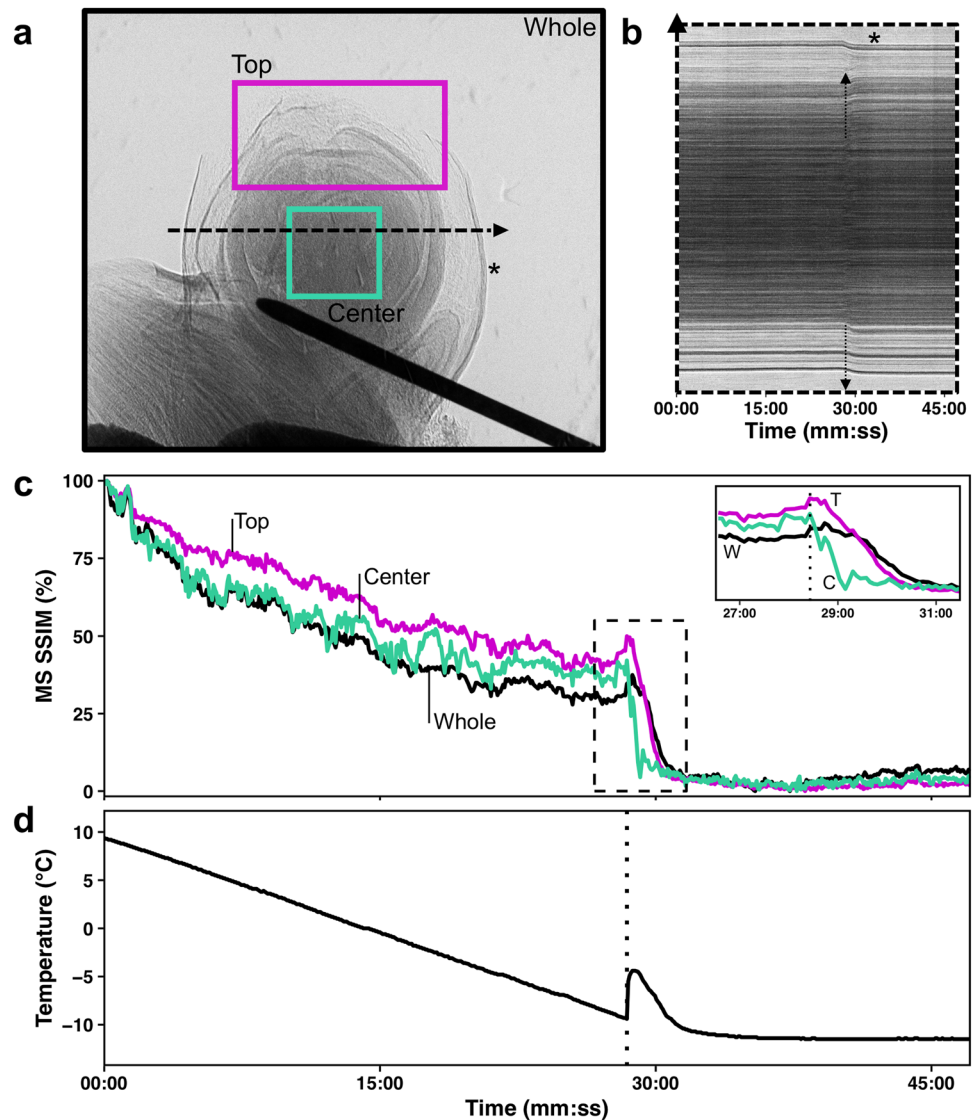


Figure 6. Characteristics of freezing in a bud of *Vitis riparia* after 11 days of deacclimation (see Supplementary Video S1). **(a)** Still image of bud at start of freezing; Black (whole image), magenta (top of the bud), and cyan (center of the bud) show areas analyzed; dashed line through center of the bud shows pixels used to build kymograph. **(b)** Kymograph resulting from line of pixels in the center of the bud; arrows show the start of freezing; asterisk marks the outer bud scale that moves inward. **(c)** Normalized multi-scale structural similarity index (MS SSIM) for three areas in (a); dashed box is shown expanded in the inset, dotted line marks the start of freezing event. **(d)** Temperature profile measured by thermocouple inside the bud; dotted line marks the start of freezing event.

Needle probe data did not show any HTEs in terms of temperature deviations from the linear rate of cooling. There were also no visible cues or MS SSIM deviations in the higher temperature region in buds imaged during cooling (Figs 6 and 7, Supplementary Videos S1–S3). In regular DTAs, HTEs are enhanced by the use of water sprays⁹, resulting in much larger peaks than LTEs. It is possible, however, that the HTE signal in non-wetted buds comes from the piece of cane attached to the bud, rather than the extracellular space in the bud itself. This agrees with the report by Neuner *et al.*⁴⁴ in the vast majority of the 37 species studied there was no ice within the buds even after HTE. HTEs may also be a result of condensation followed by freezing, or sublimation of water vapor on TEMs during the cooling in DTAs. The cryostream used in our setup has a ring of warmer, dry N₂ gas surrounding the N₂ cryostream, which prevents sublimation or condensation on the sample during the cooling. The only deviations from linear temperature change above the LTE were very slight lags in the temperature decrease (e.g., ~–10.0 °C in Fig. 7). This behavior might indicate extra-organ freezing occurs in grapevines, without extracellular ice forming within primordia such as described in other species^{35,36,53}. If the HTE happens in tissues further from the center of the bud, it is possible that the placement of the needle inserted could prevent or diminish the perception of temperature changes caused by tissues away from the center of the bud. However, LTEs corresponding to secondary buds were seen and measured based on temperature changes (Fig. 7). The lack of HTE may also

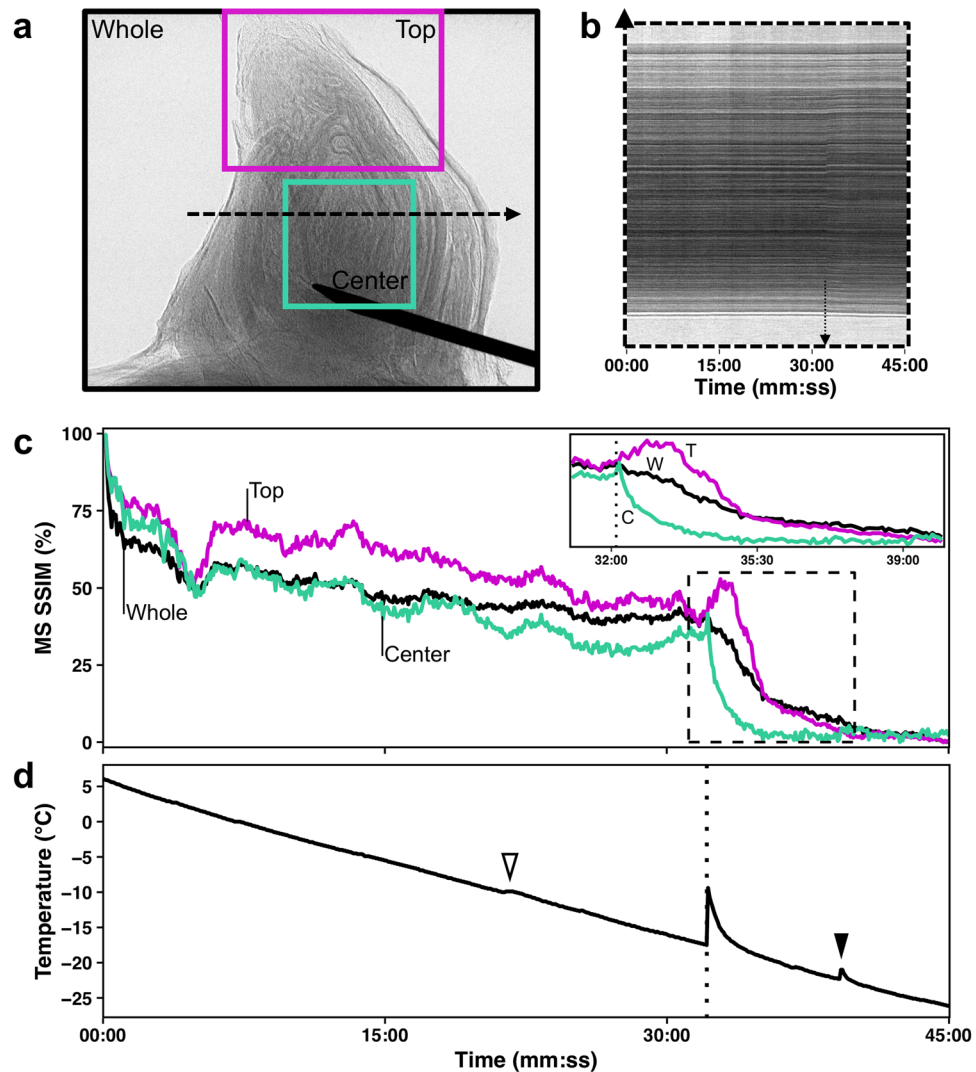


Figure 7. Characteristics of freezing in a bud of *Vitis amurensis* stored at 4 °C (see Supplementary Video S2). (a) Still image of bud at start of freezing; Black (whole image), magenta (top of the bud), and cyan (center of the bud) show areas analyzed; dashed line through center of the bud shows pixels used to build kymograph. (b) Kymograph resulting from line of pixels in the center of the bud; arrows show the start of freezing. (c) Normalized multi-scale structural similarity index (MS SSIM) for three areas in (a); dashed box is shown expanded in the inset, dotted line marks the start of freezing event. (d) Temperature profile measured by thermocouple inside the bud; dotted line marks the start of freezing event, open arrowhead shows slight lag, closed arrowhead shows secondary bud exotherm.

be an artifact of the high rate of cooling used as compared to regular DTA. However, LTEs measured were not far from expected values, and therefore HTEs may not be necessary for supercooling to occur. Further testing using multiple needles in buds should be conducted using different methods and rates of cooling to verify the occurrence, location, and importance of HTEs.

The resolution obtained in the freezing images of 2 μm pixel size was not enough to resolve ice crystals in the buds such as observed by Sinclair *et al.*⁴⁶ imaging larvae of *Chymomyza amoena* and *Drosophila melanogaster*. Larvae have free lymph in large volumes, allowing the formation of large crystals within their bodies. In grapevine buds, most of the water is located inside cells with diameter less than 20 μm . While imaging at a higher resolution ($\sim 1 \mu\text{m}$) is possible, increasing the resolution results in a smaller area of imaging¹⁹ that would likely not fit a whole bud. Therefore, we assessed freezing as the movement resulting from volume expansion due to phase change in water, also observed by Sinclair *et al.*⁴⁶ and correlated with freezing exotherms.

Despite the cryostream hitting the bud from the top, possibly generating a small temperature gradient, freezing was directly observed to occur initially from the inside, followed by outward progression in all species (Figs 6 and 7, Supplementary Videos S1–S3). Based on the MS SSIM, we can see that decay occurs earlier in the center portion vs. the top portion (Figs 6 and 7). This is also very clearly observed in Supplementary Video S2, where the *V. amurensis* bud scales located in the distal portion of the bud appear to be the last ones to freeze as they slightly unfold. This is a similar behavior to what was described by Quamme *et al.*⁵³ for buds of peach (*Prunus persica*), in

which ice propagates from the subtending tissues into the bud. Considering the apparent higher cold hardiness in bud scales compared to the shoot tip area, future studies exploring cold hardiness may want to compare these structures within the bud in terms of anatomy and gene expression.

Clear morphological differences are seen between the three species studied. *V. vinifera* has much less green (solid) tissue per bud volume than the other two species analyzed. Much of the bud volume is actually occupied by wool material (most visible in Fig. 3b,c). This adaptation is potentially linked to the region of origin: buds of *V. vinifera* likely had to adapt to reduce water loss during the dormant season in a warmer and drier place (Mediterranean) as compared to the areas where *V. amurensis* and *V. riparia* are native (Northeastern Asia and North America, respectively), and this packed tissue could help limit gas exchanges between green tissue and the atmosphere. The differences in tissue of *V. amurensis* and *V. riparia* buds compared to *V. vinifera* also validate visible differences observed during budbreak. *V. riparia* has faster early development in the E-L scale compared to *V. vinifera*, even when responses to temperature are corrected⁷. This may be a result of the larger volume of green tissue present in buds of *V. riparia* compared to *V. vinifera*. The implication of this observation is that there is less bud volume available for expanding tissues to fill in *V. riparia*, thus bud scales are forced open “earlier” in this species. Although it was not seen, *V. amurensis* would probably have similar or earlier budbreak than *V. riparia*, considering all of the tissues within the bud are extremely compacted and any expansion might result in appearance of early stages of budbreak (opening of the outer scales). It is not clear however how these morphological differences may implicate in greater maximum cold hardiness in *V. amurensis* and *V. riparia* compared to *V. vinifera*²⁷.

The increase in volume upon freezing is positively correlated with deacclimation, and faster increase of volume and deacclimation rates are seen in *V. amurensis* and *V. riparia* as compared to *V. vinifera* (Figs 1 and 5). This could indicate that increases in volume are reducing the ability of buds to supercool, likely as a result of influx of water leading to turgor⁵⁶. Although it is not known how plants are able to control levels of deep supercooling, from a physical aspect it is known that larger volumes of water are at higher risk of ice nucleation at any given temperature²⁴. Cold hardiness is correlated with bud water relations^{55,57}, and *V. vinifera* buds have an increase in ~25% water content from dormant to budbreak stage^{56,58}. However, it is important to acknowledge that metabolic changes within the bud during deacclimation can also play a part in the loss of supercooling ability^{48,58}. The more rapid increase in volume in the later stages may be a result of re-establishment of vascular connections between the bud and the cane⁵⁶. In newly developed xylem one does see large vessels as in the secondary xylem in canes, but the use of contrasting agents⁸ could be used to evaluate the formation of xylem connections such as is done with dyes and light microscopy⁵⁶. Contrasting agents may also be of potential use to more easily segment different parts of the bud in a virtual histology approach if differential uptake by tissues leads to clear density differences¹⁸, which could be tested in future assessments.

Buds took several minutes to completely freeze. This occurred despite the steep cooling rate and the cooling method based on a cryostream, which would reduce the difference in air to bud temperature by greatly decreasing the boundary layer⁵⁹. This contradicts previous descriptions that the freezing that produces an LTE is sudden²³, and lasts only a few seconds in buds of multiple species by Neuner *et al*⁴⁴. using infrared imaging for infrared DTA (IDTA). Because IDTA only observes the increase in temperature of the bud, propagating heat from the center of the bud to the outside would appear the same way as if ice was forming in those tissues. Indeed, our temperature probe data shows that the derivative of temperature measurements is only positive for a very brief period of time (Figs 6d and 7d). However, both the MS SSIM (Figs 6c and 7c) and Supplementary Videos demonstrate that the wave of bud freezing lasts longer, even as the downward trend in the temperature measurements has resumed. Such downward trend in temperature would not appear in the images from IDTA, and therefore a great portion of the time for freezing is ignored. It is also important to note that the freezing of the secondary bud in *V. amurensis* (Fig. 7; Supplementary Video S2) appears to be a separate event entirely. This suggests that the freezing of secondary buds is protected from the primaries by a barrier that is not overcome by the propagation of ice that occurs upon initial freezing.

There was a difference in the time it took to completely freeze different buds. The size difference and amount of green tissue between species and development stages might justify why some buds froze more quickly compared to the other species if a similar rate of intracellular ice growth propagation is considered⁶⁰. Although *V. amurensis* has buds with more volume than *V. vinifera*, it is possible that the wool in *V. vinifera* buds, as well as the shape of it reduced the rate of heat loss to the exterior. Energy balance studies comparing theoretical buds may allow for explanations for the differences in the duration of freezing. However, it is unlikely that insulation capabilities of bud tissues would be an adaptive response to increase cold hardiness, since air temperature changes in nature occur at a much lower rate and low temperature exposure lasts for longer periods of time.

X-ray microtomography proved to be a useful approach to identify structures within a bud, as well as for quantitative analysis of changes during loss of cold hardiness and early budbreak. Although our setup required removal of the bud from the cane, adaptation of a sample holder could lead to observation of growth in the same bud during development. Future explorations with contrasting agents⁸ may aid in anatomical studies, with special interest to water movement in the bud. High temperature exotherms were not visible or measurable, which indicates they may be an artifact of the larger sensors used in DTA. The use of 2D time-lapse X-ray phase contrast associated with a thermocouple was useful in identifying how ice spreads throughout the bud. We identified the differential response where the center of the bud is from where ice nucleates and propagates toward the scales, and showed that extra-organ freezing on scales or extracellular ice are not necessary for supercooling of buds of different grapevine species. Finally, ice propagation observed by movement of tissues occurred over several minutes.

Received: 16 July 2019; Accepted: 27 September 2019;

Published online: 18 October 2019

References

- Pratt, C. Reproductive anatomy in cultivated grapes - a review. *Am. J. Enol. Vit.* **22**, 92–109 (1971).
- Lang, G. A., Early, J. D., Martin, G. C. & Darnell, R. L. Endo-, para-, and ecodormancy: physiological terminology and classification for dormancy research. *HortSci.* **22**, 371–377 (1987).
- Londo, J. P. & Johnson, L. M. Variation in the chilling requirement and budburst rate of wild *Vitis* species. *Env. Exp. Bot.* **106**, 138–147 (2014).
- Londo, J. P. & Kovaleski, A. P. Deconstructing cold hardiness: variation in supercooling ability and chilling requirements in the wild grapevine *Vitis riparia*. *Aus. J. Grape Wine Res.* **25**, 276–285, <https://doi.org/10.1111/ajgw.12389> (2019).
- Coombe, B. G. & Iland, P. Grapevine phenology. In Dry, P. R. & Coombe, B. G., eds *Viticulture*, vol 1: Resources. Winetitles, Ashford, Australia, 210–248 (2005).
- Andreini, L., Viti, R. & Scalabrelli, G. Study on the morphological evolution of bud break in *Vitis vinifera* L. *Vitis* **48**, 153–158 (2009).
- Kovaleski, A. P., Reisch, B. I. & Londo, J. P. Deacclimation kinetics as a quantitative phenotype for delineating the dormancy transition and thermal efficiency for budbreak in *Vitis* species. *AoB PLANTS* **10**, ply066, <https://doi.org/10.1093/aob-pla/ply066> (2018).
- Staedler, Y. M., Masson, D. & Schönenberger, J. Plant tissues in 3D via X-ray tomography: simple contrasting methods allow high resolution imaging. *PLoS one* **8**, e75295 (2013).
- Mayo, S. C., Chen, F. & Evans, R. Micron-scale 3D imaging of wood and plant microstructure using high-resolution X-ray phase-contrast microtomography. *J. Str. Bio.* **171**, 182–188 (2010).
- Sedighi Gilani, M., Boone, M. N., Mader, K. & Schwarze, F. W. M. R. Synchrotron X-ray micro-tomography imaging and analysis of wood degraded by *Physisporinus vitreus* and *Xylaria longipes*. *J. Str. Bio.* **187**, 149–157 (2014).
- Cochard, H., Delzon, S. & Badel, E. X-ray microtomography (micro-CT): a reference technology for high-resolution quantification of xylem embolism in trees. *Plant, Cell & Env.* **38**, 201–206 (2015).
- Torres-Ruiz, J. M. *et al.* Direct x-ray microtomography observation confirms the induction of embolism upon xylem cutting under tension. *Plant Phys.* **167**, 40–43 (2015).
- Choat, B. *et al.* Noninvasive measurement of vulnerability to drought-induced embolism by X-ray microtomography. *Plant Phys.* **170**, 273–282 (2016).
- Malek, M., Khelifa, H., Picart, P., Mounier, D. & Poilâne, C. Microtomography imaging of an isolated plant fiber: a digital holographic approach. *Appl. Optics* **55**, A111–21 (2016).
- Nardini, A. *et al.* X-ray microtomography observations of xylem embolism in stems of *Laurus nobilis* are consistent with hydraulic measurements of percentage loss of conductance. *New Phyt.* **213**, 1068–1075 (2017).
- Scoffoni, C. *et al.* Leaf vein xylem conduit diameter influences susceptibility to embolism and hydraulic decline. *New Phyt.* **213**, 1076–1092 (2017).
- Koddenberg, T. & Miltz, H. Morphological imaging and quantification of axial xylem tissue in *Fraxinus excelsior* L. through X-ray micro-computed tomography. *Micron* **111**, 28–35 (2018).
- Rousseau, D. *et al.* Fast virtual histology using X-ray in-line phase tomography: application to the 3D anatomy of maize developing seeds. *Plant Methods* **11**, 55 (2015).
- Verboven, P. *et al.* Synchrotron X-ray computed laminography of the three-dimensional anatomy of tomato leaves. *Plant J.* **81**, 169–182 (2015).
- Tracy, S. R., Gómez, J. F., Sturrock, C. J., Wilson, Z. A. & Ferguson, A. C. Non-destructive determination of floral staging in cereals using X-ray micro computed tomography (μ CT). *Plant Methods* **13**, 9, <https://doi.org/10.1186/s13007-017-0162-x> (2017).
- Burke, M. J., Gusta, L. V., Quamme, H. A., Weiser, C. J. & Li, P. H. Freezing and injury in plants. *Annu. Rev. Plant Phys.* **27**, 507–528 (1976).
- Andrews, P. K., Sandidge, C. R. III. & Toyama, T. K. Deep supercooling of dormant and deacclimating *Vitis* buds. *Am. J. Enol. Vit.* **35**, 175–177 (1984).
- Quamme, H. A. Deep supercooling in buds of woody plants. In: *Biological ice nucleation and its applications*. 183–199 (1995).
- Bigg, E. K. The supercooling of water. *Proc. Phys. Soc. Sec. B* **66**, 688–694 (1953).
- Ferguson, J. C., Moyer, M. M., Mills, L. J., Hoogenboom, G. & Keller, M. Modeling dormant bud cold hardiness and budbreak in twenty-three *Vitis* genotypes reveals variation by region of origin. *Am. J. Enol. Vit.* **65**, 59–71 (2014).
- Ferguson, J. C., Tarara, J. M., Mills, L. J., Grove, G. G. & Keller, M. Dynamic thermal time model of cold hardiness for dormant grapevine buds. *Ann. Bot.* **107**, 389–396 (2011).
- Londo, J. P. & Kovaleski, A. P. Characterization of Wild North American Grapevine Cold Hardiness Using Differential Thermal Analysis. *Am. J. Enol. Vit.* **68**, 203–212, <https://doi.org/10.5344/ajev.2016.16090> (2017).
- Parker, J. Cold Resistance in Woody Plants. *Bot. Rev.* **29**, 123–201 (1963).
- Mills, L. J., Ferguson, J. C. & Keller, M. Cold-hardiness evaluation of grapevine buds and cane tissues. *Am. J. Enol. Vit.* **57**, 194–200 (2006).
- Molisch, H. Untersuchungen über das Erfrieren der Pflanzen (1897). Reprinted in English in *Cryo-Letters* **3**, 332–390 (1982).
- Bevilacqua, A., Zaritzky, N. E. & Calvelo, A. Histological measurements of ice in frozen beef. *J. Food Tech.* **14**, 237–251 (1979).
- Morris, G. J., Coulson, G. E. & Engels, M. A Cryomicroscopic Study of *Cylindrocystis brebissonii* De Bary and Two Species of *Micrasterias* Ralfs (Conjugatophyceae, Chlorophyta) during Freezing and Thawing. *J. Exp. Bot.* **37**, 842–856 (1986).
- Guenther, J. F. *et al.* Extra- and intra-cellular ice formation in Stage I and II *Xenopus laevis* oocytes. *Cryobiology* **52**, 401–416 (2006).
- Stott, S. L. & Karlsson, J. O. M. Visualization of intracellular ice formation using high-speed video cryomicroscopy. *Cryobiology* **58**, 84–95 (2009).
- Endoh, K., Kasuga, J., Arakawa, K., Ito, T. & Fujikawa, S. Cryo-scanning electron microscopic study on freezing behaviors of tissue cells in dormant buds of larch (*Larix kaempferi*). *Cryobiology* **59**, 214–222 (2009).
- Endoh, K., Kuwabara, C., Arakawa, K. & Fujikawa, S. Consideration of the reasons why dormant buds of trees have evolved extraorgan freezing as an adaptation for winter survival. *Env. Exp. Bot.* **106**, 52–59 (2014).
- Do, G.-S., Sagara, Y., Tabata, M., Kudoh, K.-i. & Higuchi, T. Three-dimensional measurement of ice crystals in frozen beef with a micro-slicer image processing system. *Int. J. Refrig.* **27**, 184–190, [https://doi.org/10.1016/S0140-7007\(03\)00042-2](https://doi.org/10.1016/S0140-7007(03)00042-2) (2004).
- Ishikawa, M., Price, W. S., Ide, H. & Arata, Y. Visualization of freezing behaviors in leaf and flower buds of full-moon maple by nuclear magnetic resonance microscopy. *Plant Phys.* **115**, 1515–1524 (1997).
- Kerr, W. L., Kauten, R. J., McCarthy, M. J. & Reid, D. S. Monitoring the formation of ice during food freezing by magnetic resonance imaging. *LWT - Food Sci. Tech.* **31**, 215–220 (1998).
- Wisniewski, M., Lindow, S. E. & Ashworth, E. N. Observations of ice nucleation and propagation in plants using infrared video thermography. *Plant Phys.* **113**, 327–334, <https://doi.org/10.1104/pp.113.2.327> (1997).
- Workmaster, B. A. A. & Palta, J. P. Ice nucleation and propagation in cranberry uprights and fruit using infrared video thermography. *J. Am. Soc. Hort. Sci.* **124**, 619–625 (1999).
- Bauerecker, S., Ulbig, P., Buch, V., Vrbka, L. & Jungwirth, P. Monitoring ice nucleation in pure and salty water via high-speed imaging and computer simulations. *J. Phys. Chem. C* **112**, 7631–7636 (2008).
- Livingston, D. P. 3rd *et al.* High-definition infrared thermography of ice nucleation and propagation in wheat under natural frost conditions and controlled freezing. *Planta* **247**, 791–806 (2018).

44. Neuner, G., Monitzer, K., Kaplenig, D. & Ingruber, J. Frost survival mechanism of vegetative buds in temperate trees: deep supercooling and extraorgan freezing vs. ice tolerance. *Front. Plant Sci.* **10**, 537, <https://doi.org/10.3389/fpls.2019.00537> (2019).
45. Baier-Schenk, A. *et al.* *In situ* observation of the freezing process in wheat dough by confocal laser scanning microscopy (CLSM): Formation of ice and changes in the gluten network. *J. Cereal Sci.* **42**, 255–260 (2005).
46. Sinclair, B. J. *et al.* Synchrotron x-ray visualisation of ice formation in insects during lethal and non-lethal freezing. *PLoS one* **4**, e8259 (2009).
47. Wan, Y. *et al.* A phylogenetic analysis of the grape genus (*Vitis* L.) reveals broad reticulation and concurrent diversification during Neogene and quaternary climate change. *BMC Evo. Bio.* **13**, 14 (2013).
48. Kovaleski, A. P. & Londo, J. P. Tempo of gene regulation in wild and cultivated *Vitis* species shows coordination between cold deacclimation and budbreak. *Plant Sci.* **287**, 110178 (2019).
49. Socha, J. J., Westneat, M. W., Harrison, J. E., Waters, J. S. & Lee, W.-K. Real-time phase-contrast x-ray imaging: a new technique for the study of animal form and function. *BMC Bio.* **5**, 6 (2007).
50. Lowe, D. Distinctive image features from scale-invariant keypoints. *Int. J. Comp. Vision* **60**, 91–110 (2004).
51. Schindelin, J. *et al.* Fiji: an open-source platform for biological-image analysis. *Nature Methods* **9**, 676–682, <https://doi.org/10.1038/nmeth.2019> (2012).
52. Wang, Z., Bovik, A. C., Sheikh, H. R. & Simoncelli, E. P. Image quality assessment: From error visibility to structural similarity. *IEEE Trans. Image Process.* **13**, 600–612 (2004).
53. Quamme, H. A., Su, W. A. & Veto, L. J. Anatomical features facilitating supercooling of the flower within the dormant peach flower bud. *J. Am. Soc. Hort. Sci.* **120**, 814–822 (1995).
54. Quamme, H. A. Use of thermal analysis to measure freezing resistance of grape buds. *Can. J. Plant Sci.* **66**, 947–952 (1986).
55. Ishikawa, M. & Sakai, A. Freezing avoidance mechanisms by supercooling in some *Rhododendron* flower buds with reference to water relations. *Plant & Cell Phys.* **22**, 953–967 (1981).
56. Xie, Z., Forney, C. F. & Bondada, B. Renewal of vascular connections between grapevine buds and canes during bud break. *Scientia Hort.* **233**, 331–338 (2018).
57. Richards, J. H. & Bliss, L. C. Winter water relations of a deciduous timberline conifer, *Larix laricina* Parl. *Oecologia* **69**, 16–24 (1986).
58. Meitha, K. *et al.* Developmental control of hypoxia during bud burst in grapevine. *Plant, Cell & Env.* **41**, 1154–1170 (2018).
59. Grace, J. The temperature of buds may be higher than you thought. *New Phyt.* **170**, 1–3 (2006).
60. Acker, J. P., Elliott, J. A. & McGann, L. E. Intercellular ice propagation: experimental evidence for ice growth through membrane pores. *Biophys. J.* **81**, 1389–1397 (2001).

Acknowledgements

This work is based upon research conducted at the Cornell High Energy Synchrotron Source (CHESS) which is supported by the National Science Foundation under award DMR-1332208. This work was partially supported by: CAPES, Coordenação de Aperfeiçoamento de Pessoal de Nível Superior, Brazil, award number 12945/13-7; the National Science Foundation Plant Genome Research Program Award 1546869; the Putnam Fellowship Program of the Arnold Arboretum of Harvard University; and an appointment to the Agricultural Research Service (ARS) Research Participation Program administered by the Oak Ridge Institute for Science and Education (ORISE) through an interagency agreement between the U.S. Department of Energy (DOE) and the U.S. Department of Agriculture (ORISE is managed by ORAU under DOE contract number DE-SC0014664). All opinions expressed in this paper are the authors' and do not necessarily reflect the policies and views of USDA, ARS, DOE, or ORAU/ORISE.

Author contributions

A.P.K. and J.P.L. designed the study. A.P.K. and K.D.F. collected the data. A.P.K. analyzed data. A.P.K. wrote the manuscript, and J.P.L. and K.D.F. critically revised the paper prior to submission.

Competing interests

The authors declare no competing interests.

Additional information

Supplementary information is available for this paper at <https://doi.org/10.1038/s41598-019-51415-2>.

Correspondence and requests for materials should be addressed to A.P.K. or J.P.L.

Reprints and permissions information is available at www.nature.com/reprints.

Publisher's note Springer Nature remains neutral with regard to jurisdictional claims in published maps and institutional affiliations.



Open Access This article is licensed under a Creative Commons Attribution 4.0 International License, which permits use, sharing, adaptation, distribution and reproduction in any medium or format, as long as you give appropriate credit to the original author(s) and the source, provide a link to the Creative Commons license, and indicate if changes were made. The images or other third party material in this article are included in the article's Creative Commons license, unless indicated otherwise in a credit line to the material. If material is not included in the article's Creative Commons license and your intended use is not permitted by statutory regulation or exceeds the permitted use, you will need to obtain permission directly from the copyright holder. To view a copy of this license, visit <http://creativecommons.org/licenses/by/4.0/>.

© The Author(s) 2019